Effect of Silver Electrode Wetting State on Oxygen Reduction Electrochemistry

Austin McKee[a,†], Avik Samanta[b,†], Alan Rassoolkhani[a], Jonathan Koonce[a], Wuji Huang[b], Jacob Fields[a], Scott K. Shaw[c], Joseph Gomes[a], Hongtao Ding[b,*], and Syed Mubeen[a,*]

[a] Department of Chemical and Biochemical Engineering, University of Iowa, Iowa City, IA 52242, USA

[b] Department of Mechanical Engineering, The University of Iowa, Iowa City, Iowa 52242, USA

[c] Department of Chemistry, The University of Iowa, Iowa City, Iowa 52242, USA

† Co-first Author

*Corresponding author: syed-mubeen@uiowa.edu, +1 319 335 5813

hongtao-ding@uiowa.edu, +1 319 335 5674

Title	Supplementary No.
Materials and surface processing methods	S1
Wettability measurement	S2
Characterization of surface morphology and roughness	S3
Characterization of surface chemical groups	S4
Stability of wettability	S5
Intrinsic electronic structures of Ag catalysts	S6
Mounting of silver directly to the rotating disk electrode	S7
Density functional theory calculations	S8

S1.   Materials and surface processing methhods

S1.1 Materials

Silver sheet (99.998%, 0.25mm (0.01in) thick, annealed, Premion Silver) were procured from Alfa Aesar, USA. 1H,1H,2H,2H-perfluorododecyltrichlorosilane [$CF_3(CF_2)_9(CH_2)_2SiCl_3$; FDDTS; 97%], toluene ($C_6H_5CH_3$; 99.8%) 3-cyanopropyltricholosilane [$CN(CH_2)_3SiCl_3$; CPTS; 97%] and Ethanol (C_2H_5OH; 99.5%) were procured from SigmaAldrich. Silver sheet was cut into 1 cm × 1 cm square samples. These samples underwent a polishing process to remove any surface oxides prior to surface processing.

S1.2 Nanosecond laser texturing in water confinement (wNLT)

Silver samples were textured using a Q-switched infrared Nd:YAG nanosecond pulsed laser with a pulse duration of 8 ns and repitiion rate of 10 Hz. 3.4W laser power with Gaussian distribution of laser beam intensity was used and the pulse energy was in the order of hundreds of mJ. The laser beam irradiated the silver surface in a zig-zag fashion through a galvanometer laser scanner (SCANLAB intelliSCAN® 20) configured with an f-theta objective. During the process, the silver specimens were submerged in deionized (DI) water during the process, thereby confining the laser-induced plasma and surface-enhancing effects. Details of the wNLT process parameters were listed in Table S1.

Table S1. Experimental conditions of wNLT step

Material	Laser power (W)	Pulse width (ns)	Repition rate (Hz)	Pulse Energy (mJ)	Laser spot diameter (mm)	Laser power intensity (GW/cm^2)	Line spacing (µm)	Scanning speed (mm/s)
Silver	3.4	8	10	340	3.0	0.6	1200	12.0
					1.5	2.4	600	6.0
					0.8	8.4	320	3.2
					0.3	18.2	100	1.0

S1.3 Chemical solution preparation for CIT process to achieve superhydrophobicity

0.25 grams of solid FDDTS was dissolved in 100 mL absolute toluene. The solution was stirred for 30 mins in a magnetic stirrer at room temperature to assure the solution was uniformly mixed.

S1.4 Chemical solution preparation for CIT process to achieve superhydrophilicity

1.5 mL CPTS was dissolved in 98.5 mL absolute ethanol to obtain a 100 mL solution. The solution was stirred for 30 mins in a magnetic stirrer at room temperature to assure the solution was uniformly mixed.

S1.5 Chemical immersion treatment (CIT)

After the wNLT process, the textured Ag specimens were immersed in chemical solutions at room temperature for 3 h during the CIT process to achieve the designed wettability scenarios. After 3 h, the specimens were taken out of the solution and cleaned with DI water and

subsequently dried using compressed nitrogen. After that, specimens were dried in a vacuum oven at 80 °C for 1 h.

S2. Wettability measurement

To examine the wettability of the textured silver, 5 µL volume of water was dropped using a micropipette to form a still water droplet on the specimen surface. All specimens in this example were treated using laser power intensities ranging from 0.6 to 8.4 GW/cm2 then subject to CIT processing using an FDDTS reagent. All specimens achieved hydrophobicity with θ_w greater than 90°. Tuneable hydrophobicity, characterized by a contact angle ranging between 90° to 136°, can also be achieved by carefully controlling the laser power intensity. Similarly, surfaces subject to laser power intensities 0.6 to 18.2 GW/cm^2 and subsequent CIT process using a CPTS reagent achieved hydrophilicity with θ_w less than 90°. By controlling laser power intensity, tuneable hydrophilicity can be achieved over a contact angle range of 30° to 90°.

S3. Characterization of surface morphology and roughness

Surface morphology of the treated surfaces was examined using Hitachi S-4800 scanning electron microscopy (SEM). Surface roughness of the treated sample was examined by a non-contact 3D optical white light interferometer (Wyko NT1100). Nine measurements were taken across different locations of the samples and average roughness is reported.

S4. Characterization of surface chemical groups

The surface chemistry was analyzed using a Kratos Axis ultrahigh-performance X-ray photoelectron spectroscopy (XPS) system. The XPS system used an incident radiation of monochromatic Al Kα X-ray (1486.6 eV) excitation source projected at 45° to sample surface. During the analysis, an accelerating voltage 15 kV and emission current 10 mA was used, and the photoelectron emitted from the surface was acquired at a takeoff angle of 90°. An ultra-high vacuum (10−9 torr) pressure was set inside the XPS chamber and the charge neutralizer was on during the analysis. Both survey spectrum analysis and core-level spectrum analysis have been performed. Survey spectrum analysis was performed over the binding energy range of 1200 eV to 5 eV using 160 eV pass energy, 1.0 eV incremental step and 200 ms dwell time. Core level spectrum analysis was performed with 20 eV pass energy, 0.1 eV incremental step and 2000 ms dwell time. After the XPS measurements, CasaXPS software was used for the spectra analysis. Shirley background and Gaussian/Lorentzian line shape were used as they are the most common method to deal with photoelectron peaks of polymers. Both survey and core-level spectra were calibrated with respect to the C 1s peak at 285.0 eV.

S5. Stability of wettability

Silver is an electronegative metal, and it is intrinsically hydrophilic.[1,2] The untreated surface had a θ_w of 51°± 6°, and it did not vary significantly over a period of 60 days in atmospheric condition. On the other hand, the wettability condition of the only laser textured surface was not stable. Immediately after laser texturing in water confinement using 8.4 GW/cm^2 laser intensity, the treated surface performed as hydrophilic with $\theta_w = 40°± 1.6°$. Upon exposure to ambient conditions, the θ_w started to increase, and it became 86°± 0.6° after 60 days, as shown in Fig. 1i. Laser textured metal surfaces adsorbed those organic constituents found in earth's atmosphere, including long-chain hydrocarbons with carbonyl groups, carboxylic acids, and diol groups,[3]

leading to wettability transition from hydrophilicity to hydrophobicity.[4] With the CIT treatment, the wettability of laser textured silver surfaces stabilizes.

S6. Intrinsic electronic structures of Ag catalysts

XPS analysis shows Ag $3d_{5/2}$, and Ag $3d_{3/2}$ core level binding energies on the untreated, hydrophilic and hydrophobic Ag catalysts 368.1 and 374.1 eV, respectively, which is in good agreement with the binding energy of Ag^0 (Supplementary Fig. 3).[5] Silver oxide states corresponding to AgO at Ag $3d_{5/2}$ = 367.33 eV for AgO[6] and 367.62 eV for Ag_2O[7] could not be found in the core-level analysis of all three samples. The presence of no silver oxide is attributed to the surface processing by pulsed laser where the Ag substrate is exposed to a very short exposure of laser irradiation (8 ns) underwater confinement. Therefore, the heating and cooling times between laser pulses are on the order of few microseconds to nanoseconds.[8] Consequently, the nanostructure generation through melting and condensation of Ag substrate was achieved within that short exposure time. The short exposure time plays a major factor in averting the formation of silver oxides.[9] Additionally, no peak is found corresponding to Ag-C bonds[5] in the three samples. As there is no formation of bonding between carbon from CPTS and FDDTS molecules with laser-treated Ag, no Ag-C bond was formed.

S7. Mounting of silver directly to the rotating disk electrode

Silver samples were cut using a metal punch making contact with the non-treated side to create disks with diameters of five centimeters. These disks were then attached to a glassy carbon rotating disk electrode with a diameter of three centimeters using Scanning Eletron Microscopy grade silver paste which was allowed to dry completely for a minimum of twelve hours. The mounted sample then had an acrylic fast-drying polymeric liquid applied around the exterior of the silver disk and on the rotating disk electrode to cover the edges of the silver disk and to create a polymer ring of approximately the same thickness as the disk.

S8. Density functional theory calculations

Density functional theory (DFT) calculations were performed to investigate the competition between $2e^-$ and $4e^-$ reaction pathways as surface wettability is modified. The density functional theory (DFT) calculations were performed using the Quantum Espresso code.[5] The electron-ion interactions were described using the projector augmented wave method.[6] The Perdew-Burke-Ernzerhof (PBE) functional[7] within the generalized gradient approximation was used to describe the electronic exchange-correlation interactions. A 3x3 Ag(111) four layer slab model was used for all DFT calculations. A 7x7x1 Monkhorst-Pack k-point grid was used to perform Brillouin zone sampling. The convergence of energy and forces were set to 10^{-5} eV and 10^{-2} eV/Å, respectively. A kinetic energy cutoff for wavefunctions was set to 680 eV. A 20 Å vacuum space was used between slabs along the Z-axis. The bottom two layers of the slab were held fixed in their bulk positions, while the top two layers and adsorbates were fully relaxed. All calculations were performed with spin-polarization.

The reaction free energy of these elementary steps was determined by the computational hydrogen electrode method proposed by Nørskov and co-workers.[8] The expressions for the adsorption free energy of reactant and product molecules are given by

$$\Delta G_{ads} = \Delta E_{ads} + \Delta E_{ZPE} - T\Delta S$$

where ΔE_{ads} is the binding energy of adsorption, ΔE_{ZPE} is the zero-point energy of each adsorbate or free molecule, T is temperature, and ΔS is the entropy change. Entropy values of gas phase molecules can be obtained from standard tables, and the entropies of adsorbed species and the adsorption site are neglected.

The adsorption free energy of the O_{ads} and OOH_{ads} can be expressed as

$$\Delta G_O = \Delta G[H_2O(g) + * \rightarrow O^* + H_2(g)]$$
$$= (E_{O*} + E_{H_2} - E_{H_2O} - E_*) + (E_{ZPE(O*)} + E_{ZPE(H_2)} - E_{ZPE(H_2O)} - E_{ZPE(*)})$$
$$-T(S_{O*} + S_{H_2} - S_{H_2O} - S_*)$$

$$\Delta G_{OOH} = \Delta G\left[2H_2O(g) + * \rightarrow OOH^* + \frac{3}{2}H_2(g)\right]$$
$$= \left(E_{OOH*} + \frac{3}{2}E_{H_2} - 2E_{H_2O} - E_*\right) + \left(E_{ZPE(OOH*)} + \frac{3}{2}E_{ZPE(H_2)} - 2E_{ZPE(H_2O)} - E_{ZPE(*)}\right)$$
$$-T(S_{OOH*} + \frac{3}{2}S_{H_2} - 2S_{H_2O} - S_*)$$

The contribution from solvation to the reactions involving aqueous phase species, OH⁻(aq) and OOH⁻(aq), were accounted by adding the difference in free energy between the gas-phase state and the aqueous-phase state. For potential-dependent elementary steps involving n-electron transfer, the free energy change at potential U was shifted by +neU with respect to that at zero potential (U = -1.0 V). To take into account the effect of electrolyte (0.1 M NaOH, pH 13), we correct the free energy of H+ ions by the concentration dependence of the entropy: $G(pH) = pH * kT ln10$, where k is the Boltzmann constant and T is temperature.

We consider the proposed product pathway for the hydrophilic surface (2e⁻) and super hydrophilic surface (4e⁻) (see Figure 3b). These reaction pathways involve a common reaction intermediate, OOH_{ads}. The selectivity determining step is one of two elementary reactions with the minimum reaction free energy,

$$OOH_{ads} + e^- \rightarrow OOH^-(aq) \ (1)$$
$$OOH_{ads} + e^- \rightarrow O_{ads} + OH^-(aq) \ (2).$$
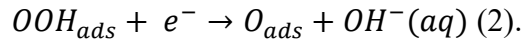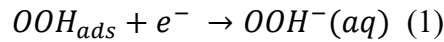
To model the effects of increasing hydrophilicity, we included explicit water molecules adsorbed on the surface alongside the reaction intermediates. We construct a ice-like water bilayer by a honeycomb ($\sqrt{3}$ x $\sqrt{3}$) R30 pattern with a 2/3 monolayer (ML) of water coverage as a model of the super hydrophilic surface. We then construct a water bilayer with a 1/3 ML of water coverage by removing half of the water molecules as a model of the hydrophilic surface.

On the super hydrophilic surface, it was found that the 4e⁻ pathway is favored ($\Delta G_{1,(2/3ML)}$ =+0.35 eV, $\Delta G_{2,(2/3ML)}$ = -1.34 eV), in good agreement with experimental observations. At lower water coverage, on the hydrophilic surface, the binding energy of all intermediates decrease. Due to the relatively weak binding of intermediates by the Ag(111) surface, the hydrogen bond network of the water bilayer plays an important role in the stabilization of species on the surface. The disruption of this hydrogen bonding network affects O_{ads} and OOH_{ads} to varying degree. While it was found that the 4e⁻ pathway is still favored on the hydrophilic surface ($\Delta G_{2,(2/3ML)}$ = -0.27 eV), the 2e⁻ pathway becomes competitive ($\Delta G_{1,(2/3ML)}$ = -0.15 eV). This indicates that both 4e⁻ and 2e⁻ product pathways could contribute to the overall reaction rate at moderate hydrophilicity.
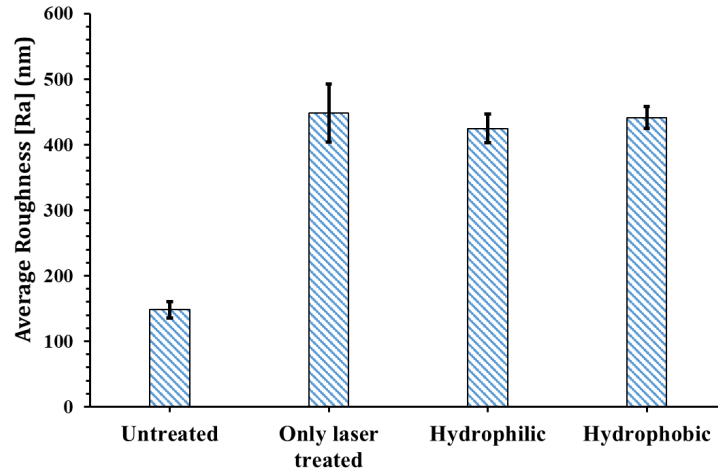
Supplemental Fig. 1. Nanoscale roughness variation untreated, only laser treated (8.4 GW/cm^2), hydrophilic (8.4 GW/cm^2)and hydrophobic Ag (8.4 GW/cm^2).
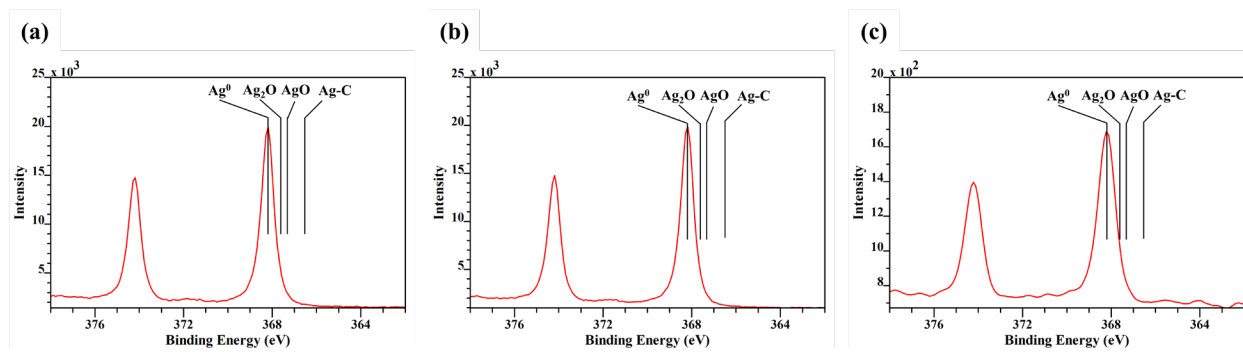
Supplemental Fig. 2. XPS Ag 3d-spectra for a) Untreated b) Hydrophilic, c) Hydrophobic.

(a)


(b)

(c)

(d)
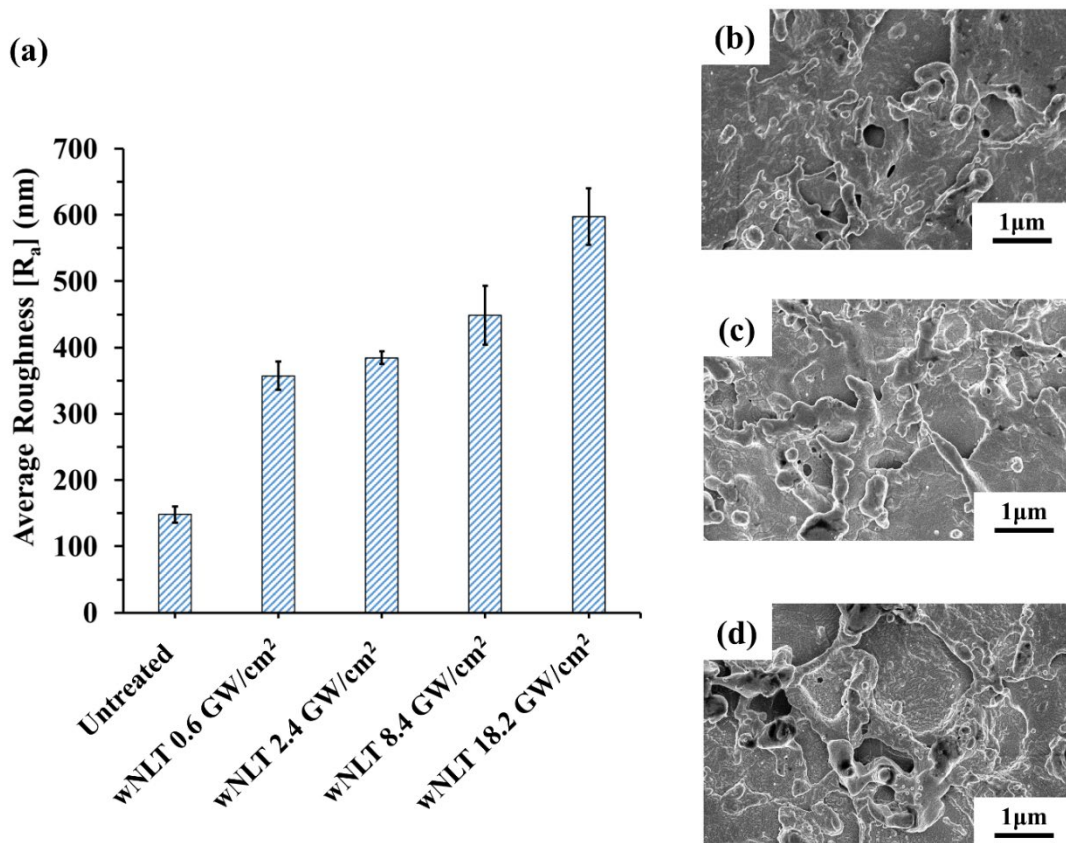
Supplemental Fig. 3. a) Nanoscale roughness variation with different laser power intensity and comparison of surface morphology of Ag samples processed with b) 2.4 GW/cm^2, c) 8.4 GW/cm^2 and d) 18.2 GW/cm^2.
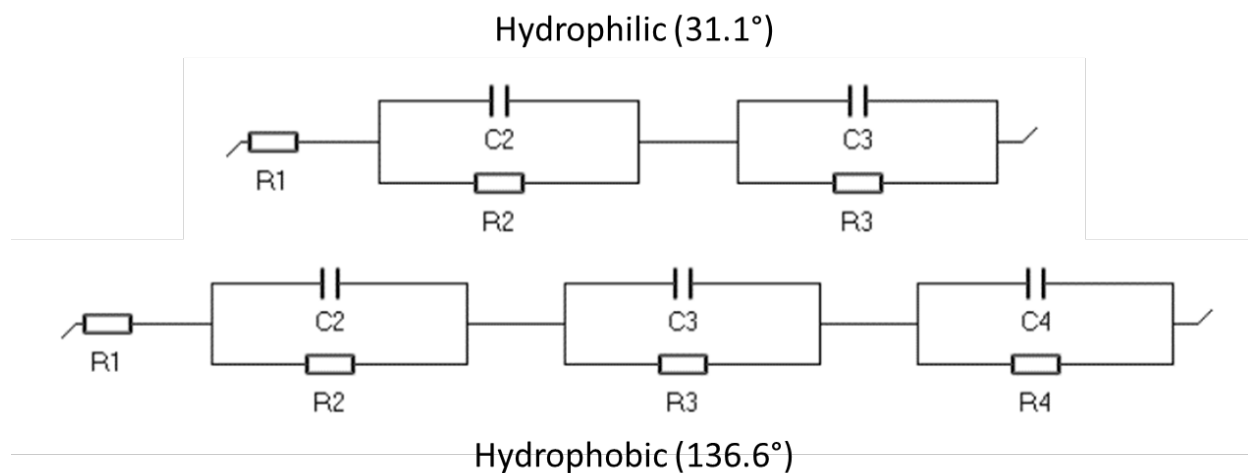
Supplemental Fig. 4. Simplified circuit models for the EIS measurements discussed and shown in Fig 2c, where R1 is the circuit resistance between the working and reference electrode, R2 is R_{ct}, R3 is R_{O2}, and R4 is R_{OH^-} and C2, C3, and C4 are the capacitances related to their equivalent resistance values.
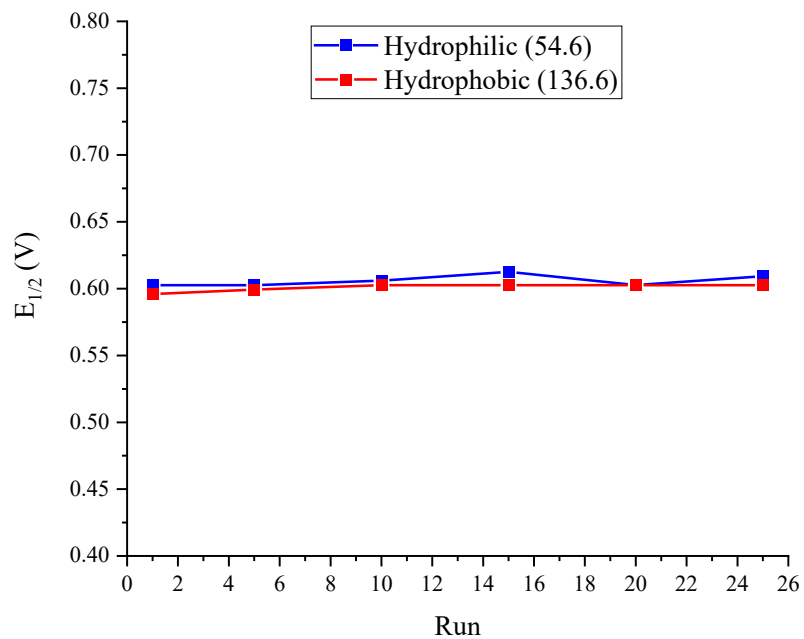
Supplemental Fig. 5. Half-wave potentials of a 25 continuous run LSV showing sample stability for approximately 2 hours of electrochemical reduction with little to no change in sample productivity or effectiveness.
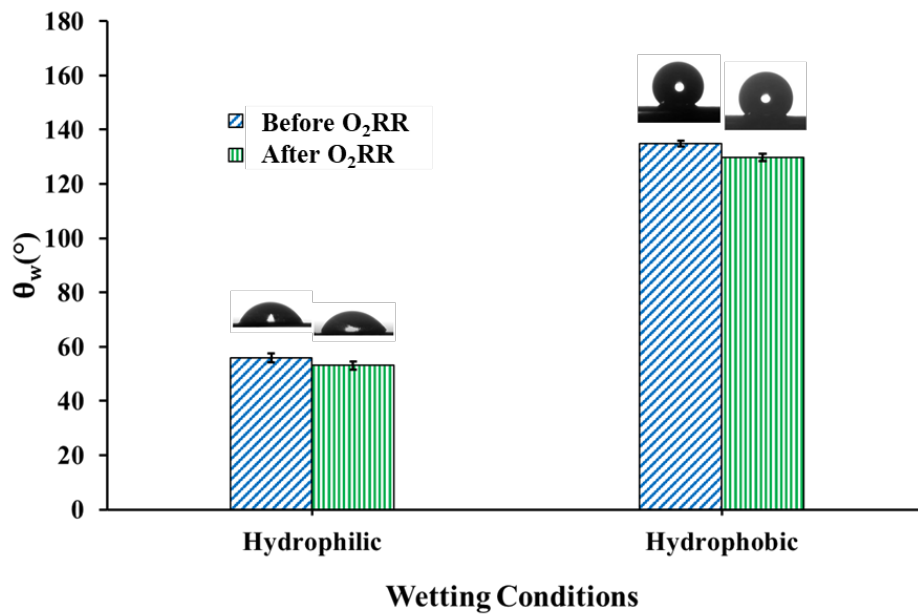
Supplemental Fig. 6. Stability of samples shown through contact angles before and after approximately 2 hours of continuous electrochemical reduction
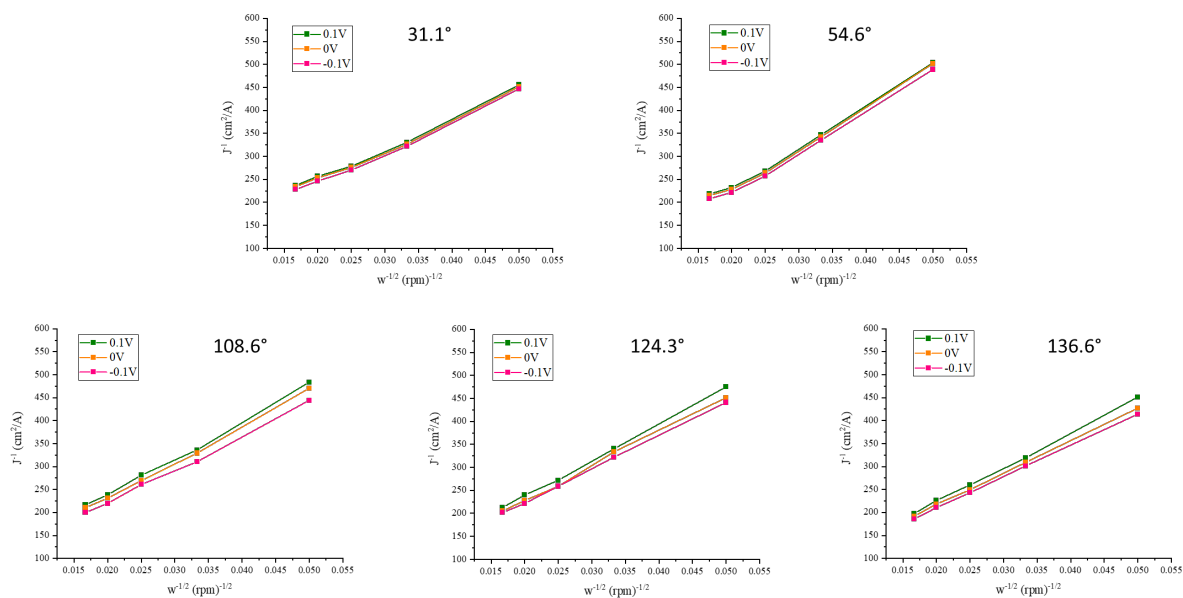
Supplemental Fig. 7. Koutecký–Levich plots constructed for RPM's 400, 900, 1600, 2500, and 3600 and voltages 0.1V, 0.0V, and -0.1V vs RHE used for product electron values
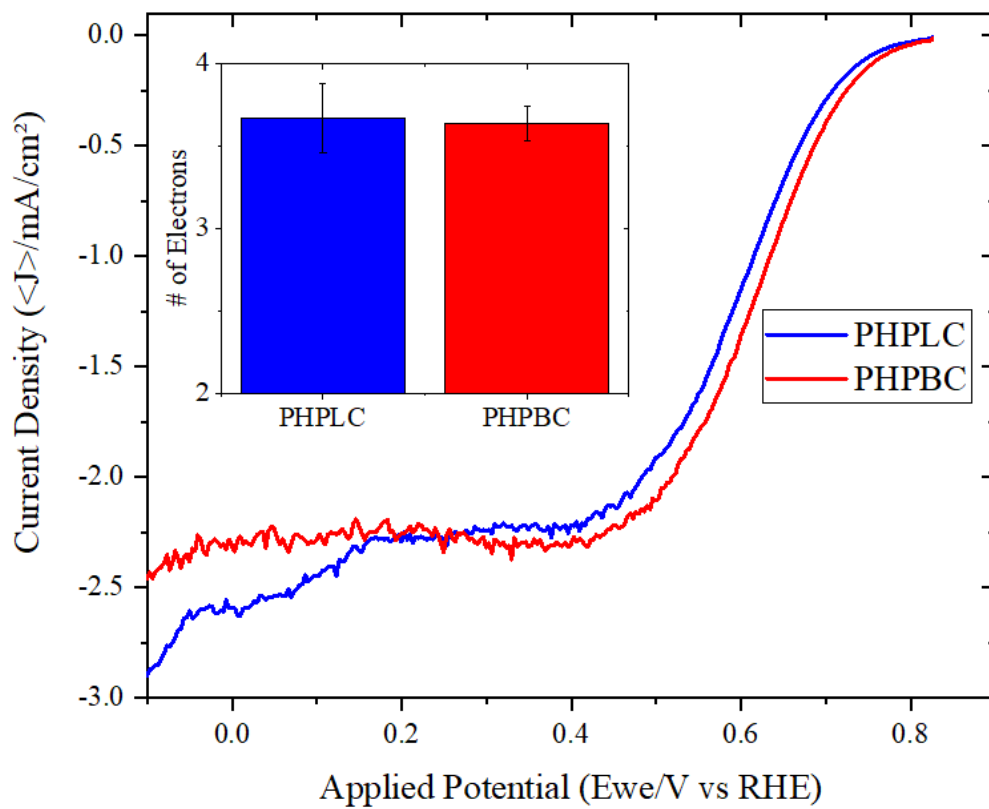
Supplemental Fig. 8. Linear Sweep Voltametry of Planar samples after chemical treatment (Planar Hydrophilic Treatment – Blue, Planar Hydrophobic Treatment – Red) with an insert of the number of electrons used in the ORR process.

References

(1) Osman, M. A.; Keller, B. A. Wettability of Native Silver Surfaces. *Appl. Surf. Sci.* **1996**, *99* (3), 261–263. https://doi.org/10.1016/0169-4332(96)00101-8.

(2) Valette, G. Hydrophilicity of Metal Surfaces. Silver, Gold and Copper Electrodes. *J. Electroanal. Chem. Interfacial Electrochem.* **1982**, *139* (2), 285–301. https://doi.org/10.1016/0022-0728(82)85127-9.

(3) Goldstein, A. H.; Galbally, I. E. Known and Unexplored Organic Constituents in the Earth's Atmosphere. *Environ. Sci. Technol.* **2007**, *41* (5), 1514–1521. https://doi.org/10.1021/es072476p.

(4) Long, J.; Zhong, M.; Zhang, H.; Fan, P. Superhydrophilicity to Superhydrophobicity Transition of Picosecond Laser Microstructured Aluminum in Ambient Air. *J. Colloid Interface Sci.* **2015**, *441*, 1–9. https://doi.org/10.1016/j.jcis.2014.11.015.

(5) Boukhvalov, D.W.; Zhidkov, I.S.; Kurmaev, E.Z.; Fazio, E.; Cholakh, S.O.; D'Urso, L. Atomic and electronic structures of stable linear carbon chains on Ag-nanoparticles. *Carbon.* **2018**, 128, 296-301. https://doi.org/10.1016/j.carbon.2017.11.044

(6) Kaspar, T.C.; Droubay, T.; Chambers, S.A.; Bagus, P.S. Spectroscopic evidence for Ag (III) in highly oxidized silver films by X-ray photoelectron spectroscopy. *J. Phys. Chem. C.* **2010**, 114, 21562-21571. https://doi.org/10.1021/jp107914e

(7) Weaver, J.F.; Hoflund, G.B. Surface characterization study of the thermal decomposition of Ag_2O, *Chem. Mater.* **1994**, 6, 1693-1699. https://doi.org/10.1021/cm00046a022

(8) Henley, S. J.; Carey, J. D.; Silva, S. R. P. Pulsed-laser-induced nanoscale island formation in thin metal-on-oxide films. *Phys. Rev. B,* **2005**, 72, 195408. https://doi.org/10.1103/PhysRevB.72.195408

(9) Oh, H.; Lee, J.; Lee, M. Transformation of silver nanowires into nanoparticles by Rayleigh instability: Comparison between laser irradiation and heat treatment. *Appl. Surf. Sci.* **2018**, *427*, 65–73. http://dx.doi.org/10.1016/j.apsusc.2017.08.102